Journal of Advanced Research 31 (2021) 1–12

Contents lists available at ScienceDirect

Journal of Advanced Research

journal homepage: www.elsevier.com/locate/jare

Lung but not brain cancer cell malignancy inhibited by commonly used anesthetic propofol during surgery: Implication of reducing cancer recurrence risk

Cong Hu [a,b], Masae Iwasaki [b,c], Zhigang Liu [d], Bincheng Wang [b], Xiaomeng Li [b], Han Lin [a], Jun Li [a], Jia V. Li [d,1], Qingquan Lian [a,*,1], Daqing Ma [b,*,1]

[a] Department of Anesthesiology, The Second Affiliated Hospital and Yuying Children's Hospital of Wenzhou Medical University, Wenzhou, Zhejiang 325027, China
[b] Division of Anaesthetics, Pain Medicine and Intensive Care, Department of Surgery and Cancer, Faculty of Medicine, Imperial College London, Chelsea & Westminster Hospital, London SW10 9NH, United Kingdom
[c] Department of Anesthesiology and Pain Medicine, Graduate School of Medicine, Nippon Medical School, Tokyo 113-8602, Japan
[d] Department of Metabolism, Digestion and Reproduction, Faculty of Medicine, Imperial College London, London SW7 2AZ, United Kingdom

GRAPHICAL ABSTRACT

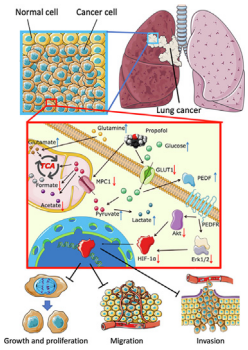

ARTICLE INFO

Article history:
Received 26 August 2020
Revised 27 October 2020
Accepted 12 December 2020
Available online 6 January 2021

Keywords:
Intravenous anesthetic
Lung cancer
Brain cancer
PEDF

ABSTRACT

Introduction: Intravenous anesthesia with propofol was reported to improve cancer surgical outcomes when compared with inhalational anesthesia. However, the underlying molecular mechanisms largely remain unknown.
Objectives: The anti-tumor effects of propofol and the possible underlying mechanism including altered metabolic and signaling pathways were studied in the current study.
Methods: The cell viability, proliferation, migration, and invasion of cancer cells were analyzed with CCK-8, Ki-67 staining, wound healing, and Transwell assay, respectively. The protein changes were analyzed with Western blot and immunofluorescent staining. The metabolomics alteration was studied with ^{1}H-NMR spectroscopy. The gene expression regulations were analyzed with PCR gene array and qRT-PCR experiments.

Peer review under responsibility of Cairo University.

* Corresponding authors at: Department of Surgery and Cancer, Faculty of Medicine, Imperial College London, Chelsea & Westminster Hospital, SW10 9NH London, United Kingdom (D. Ma) and Department of Anesthesiology, The 2nd Affiliated Hospital and Yuying Children's Hospital of Wenzhou Medical University, 325027 Wenzhou, Zhejiang, P. R. China (Q.Q. Lian).
E-mail addresses: wzmzlqq@163.com (Q. Lian), d.ma@imperial.ac.uk (D. Ma).
[1] QL, JVL and DM share the senior authorship.

https://doi.org/10.1016/j.jare.2020.12.007

HIF-1α

Results: In this study, we found that propofol reduced cell viability and inhibited cell proliferation, migration and invasion of lung cancer cells, but not neuroglioma cells. In lung cancer cells, propofol downregulated glucose transporter 1 (GLUT1), mitochondrial pyruvate carrier 1 (MPC1), p-Akt, p-Erk1/2, and hypoxia- inducible factor 1 alpha (HIF-1 α) expressions and upregulated pigment epithelium-derived factor (PEDF) expression. Propofol increased intracellular glutamate and glycine but decreased acetate and formate whilst increased glucose, lactate, glutamine, succinate, pyruvate, arginine, valine, isoleucine, and leucine and glycerol, and decreased acetate, ethanol, isopropanol in the culture media of lung cancer cells. Furthermore, VEGFA, CTBP1, CST7, CTSK, CXCL12, and CXCR4 gene expressions were downregulated, while NR4A3, RB1, NME1, MTSS1, NME4, SYK, APC, and FAT1 were upregulated following the propofol treatment. Consistent with the phenotypical changes, these molecular and metabolic changes were not found in the neuroglioma cells.

Conclusion: Our findings indicated anti-tumor effects of propofol on the lung cancer but not brain cancer, through the regulation of tumor metastasis-related genes, multi-cellular signaling and cellular metabolism.

Introduction

Cancer is the second leading disease of death worldwide [1,2]. Owing to ageing population globally, the incidence of cancer is increasing [2]. Among all the types of cancers, lung cancer caused the highest mortality in adults reported in 2017 [3], whilst in children, the mortality of brain tumor is higher than other cancer types [4].

Surgery remains the primary therapy for solid organ cancer including lung cancer [5,6]. However, most cancer patients after surgery die due to the metastasis and recurrence. Recurrence can be local, regional and distant recurrence [7], and the recurrence type, severity, and incidence are determined by many factors, including malignancy of cancer, surgical trauma and stress, adjuvant therapies and beyond [8].

It has been recognized that anesthetics and techniques may also contribute to the outcomes of cancer patients after surgery. For example, it was reported that patients received inhalational anesthetics had a shorter recurrent free life when compared to those who were administered with intravenous anesthetic propofol during their surgical treatments for cancer [9]. However, the mechanisms underlying these clinical findings remain unknown. A previous study demonstrated volatile anesthetics, such as, sevoflurane, isoflurane, and desflurane, upregulated the metastatic genes in ovarian cancer cells [10]. Furthermore, unlike propofol, isoflurane was also demonstrated to increase hypoxia-inducible factor-1 alpha (HIF-1α) [11], which is a transcriptional factor associated with the progression of a variety of cancer types, such as breast, colonic and lung cancer [12]. HIF-1α can be activated by its upstream effectors, such as Akt and Erk1/2 [13,14]. Akt, also known as protein kinase B, belongs to the cAMP-dependent protein kinase superfamily, which is involved in many biological functions, for example, cell cycle, nutrient metabolism, and transcriptional regulation [15]. Erk1/2 is also involved in a variety of biological functions, including proliferation, differentiation and cell survival [16]. Akt and Erk1/2 signaling pathways can be regulated by a diversity of factors, such as pigment epithelium-derived factor (PEDF) [17,18]. PEDF is a secreted protein of serine protease inhibitor family and has anti-angiogenic, anti-tumor, and neurotrophic functions; and its therapeutic value for heart disease, choroidal neovascularization and cancer has been explored [19,20].

In the current study, the role of PEDF and HIF-1α in anti-cancer property of propofol will be determined in lung and brain cancer cell cultures. We hypothesized that propofol downregulates glucose transporter 1 (GLUT1) and mitochondrial pyruvate carrier 1 (MPC1, also called BRP44L, brain protein 44-like) expressions, which leads to the disturbance of metabolisms of cancer cells. These changes may alter PEDF expression, which in turn, downregulates HIF-1α expression *via* Akt and Erk1/2 cellular signaling pathways. The suppression of HIF-1α expression finally affects tumor-related gene expressions and changes cancer cell malignancy and biology.

Materials and methods

Cell culture

Lung cancer (A549) and neuroglioma (H4) cell lines were obtained from ECACC (Wiltshire, UK). A549 cell line was grown in Gibco RPMI media 1640 (ThermoFisher, Paisley, UK) supplemented with 10% fetal bovine serum (FBS) and 1% penicillin–streptomycin (ThermoFisher, Paisley, UK), while H4 cell line was cultured in Gibco Dulbecco's Modified Eagle Medium (ThermoFisher, Paisley, UK) supplemented with 10% FBS and 1% penicillin–streptomycin. A549 and H4 cells were cultured at 37 °C with 5% CO_2 and balanced with air. Cells were treated with 4 μg/mL propofol (Sigma-Aldrich, Dorset, UK) for 2 h when the seeded cells formed a continuous monolayer. Intralipid (Santa Cruz Biotechnology, Dallas, Texas, USA) was used as vehicle control. After which, cell media was replaced with fresh media for the next 24 h for further experiments.

Cell counting kit-8 viability assay

The cultured A549 and H4 cells were added with cell counting kit-8 (CCK-8) solution (Sigma-Aldrich, Dorset, UK). The blank well was with media and cell counting kit-8 solution but without cells. Cancer cells were incubated at 37 °C with 5% CO_2 for 2 h. The optical density (OD) values were obtained *via* a microplate reader (Bio-Tek, Swindon, UK) at 450 nm wavelength. The cell viability was calculated as: [OD (Test) - OD (Blank)]/[OD (Control) - OD (Blank)] X 100%.

Wound healing scratch migration assay

Cancer cells were scratched in the center of the confluent monolayer and taken a picture under microscope as the baseline. The cells were incubated in media without FBS for 24 h, after which the picture was taken again at the same region. The percentage of scratching gap closure was analyzed with ImageJ 2.0 (National Institutes of Health, Bethesda, Maryland, USA).

Transwell invasion assay

Cells were collected after the dissociation by trypsin (Sigma-Aldrich, Dorset, UK). They were re-suspended with serum-free

media and seeded into the upper chamber of the Transwell assay kit (Sigma-Aldrich, Dorset, UK), which was pre-embedded with Matrigel (Sigma-Aldrich, Dorset, UK) while the lower chamber was filled with serum-enriched media. After incubation for 24 h, the upper chamber was fixed in 70% methanol for 30 min, which was followed by 15 min staining with 0.1% crystal violet (Sigma-Aldrich, Dorset, UK). After removal of the cells on the upper membrane, the cells remained on the bottom membrane were identified as invasive cells.

Immunofluorescent staining for protein expression and/or Ki-67 cell proliferation

A549 and H4 cells were fixed with 4% paraformaldehyde solution in PBS (Santa Cruz Biotechnology, Dallas, Texas, USA) for 15 min, which was followed by the blocking procedure with 10% normal donkey serum (Sigma-Aldrich, Dorset, UK) for 30 min. After blocking, they were incubated with the primary antibodies (**Table S1**) at 4 °C overnight and then probed with the secondary antibodies (**Table S1**). The cells were mounted with DAPI (4′, 6-diamidino-2-phenylindole) mounting media (Vector Laboratories, Burlingame, California, USA), and imaged by fluorescent microscopy. ImageJ 2.0 software (National Institutes of Health, Bethesda, Maryland, USA) was used to quantify analysis wherever necessary.

Western blotting determining protein expression

Western blotting was done using our established protocol [10]. The treated cells were lysed in cell lysis buffer (Cell Signaling, Danvers, Massachusetts, USA) and the protein concentration of the supernatant sample of cell lysis was measured. Protein samples with 60 μg were loaded into 4–12% polyacrylamide gel (Life Technologies, Paisley, UK) to be electrophoresed for 1.5 h. After transferring the protein bands onto a polyvinylidene difluoride (PVDF) membrane, the membrane was blocked with 5% non-fat milk for 1 h, before incubation with the primary antibodies (**Table S1**) at 4 °C overnight. After washing, the membrane was incubated with the secondary antibodies (**Table S1**) for 1 h at room temperature. The membrane was immersed with the enhanced chemiluminescence (ECL) system (Santa Cruz Biotechnology, Dallas, Texas, USA), and developed by GeneSnap (Syngene, Cambridge, UK). The intensity of blot bands was quantified with ImageJ 2.0 (National Institutes of Health, Bethesda, Maryland, USA).

Nuclear magnetic resonance spectroscopic analysis of cells and media

Cell pellets were collected with trypsin (Sigma-Aldrich, Dorset, UK) and placed into a bead beater tube (STARLAB Science Laboratory, Hamburg, Germany) containing 0.1 g sterile beads with a diameter of 0.1 mm and 1.5 mL of the pre-chilled mixture of methanol (Thermo Fisher, Paisley, UK) and water (MeOH:H_2O, v:v, 1:1). The tubes were placed in a bead beater (Bertin Instruments, Montigny-le-Bretonneux, France) to homogenize the samples using two cycles of 6,500 Hz for 40 s with 5 min on dry ice between cycles. The samples were then centrifuged at 10,000 *g* at 4 °C for 10 min and the supernatants were transferred to new Eppendorf tubes before drying at 45 °C overnight and stored at −40 °C. The dry cell extract samples were resuspended in 210 μL of potassium phosphate buffer (pH = 7.4) containing deuterium oxide (D_2O) for magnetic field lock, 0.01% 3-(trimethylsilyl)-[2,2,3,3-$^2H_4$]-propionic acid sodium salt (TSP) for the spectral calibration, 0.15 M KH_2PO_4, and 0.1 mM sodium azide (NaN_3). The resulting mixture was centrifuged at 20,817 *g* for 10 min, and 180 μL supernatant was transferred to an NMR tube (Bruker Corporation, Rheinstetten, Germany) with an outer diameter of 3 mm pending ^{1}H-NMR spectral acquisition.

The cell media were collected and centrifuged at 18,000 *g* for 10 min. A total of 540 μL supernatant was mixed with 60 μL potassium phosphate buffer containing D_2O, 0.1% TSP, 1.5 M KH_2PO_4 and 1 mM NaN_3. The mixture was transferred to an NMR tube with an outer diameter of 5 mm pending ^{1}H NMR spectral acquisition.

The ^{1}H-NMR spectra of cell extract and media samples were obtained using a Bruker 600 MHz spectrometer (Bruker Corporation, Rheinstetten, Germany) at the operating ^{1}H frequency of 600.13 MHz at a temperature of 300 K. A standard NMR pulse sequence (recycle delay-90°-t_1-90°-t_m-90° acquisition) was applied to acquire ^{1}H NMR spectral data (t_1 = 3 μs, t_m = 100 ms). The water peak suppression was achieved using selective irradiation during a recycle delay of 4 s and t_m. A 90° pulse was adjusted to ~ 10 μs. A total of 32 scans were collected into 64 k data points with a spectral width of 20 ppm.

PCR gene array

RNeasy mini kit® and QIAshredder (QIAGEN, West Sussex, UK) were employed to obtain total RNA from cells. A BioPhotometer (Eppendorf, Stevenage, UK) was used to determine the quantity and quality of RNA. The A260/A280 and A260/A230 ratio greater than 1.8 and 1.7 respectively, were regarded as sufficient quality for further analysis. The RT^2 First Strand Kit (QIAGEN, West Sussex, UK) was utilized to convert total RNA to complementary DNA (cDNA), which was then mixed with SYBR Green ROX FAST Mastermix (QIAGEN, West Sussex, UK). The mixture was added in an RT^2 Profiler™ PCR Array Human Tumor Metastasis (QIAGEN, West Sussex, UK), which was processed and analyzed with the Rotor-Gene Q system (QIAGEN, West Sussex, UK).

qRT-PCR determining gene expression

Paired oligonucleotide forward and reverse primers (**Table S2**) for C-X-C chemokine receptor type 4 (*CXCR4*) and *GAPDH* were designed using Primer Designer (Scientific and Educational Software, Durham, USA) against the sequence downloaded from GenBank and obtained from Invitrogen. The process of RNA extraction and cDNA generation was the same as those in the PCR array experiment. The cDNA sample was mixed with forward and reverse primers and SYBR Green ROX qPCR Mastermix (QIAGEN, West Sussex, UK). The PCR mixture was processed and analyzed with the Rotor-Gene Q system (QIAGEN, West Sussex, UK). All mRNA data were expressed relative to the endogenous control gene, GAPDH.

Statistical analysis

Data were expressed as median (range) or mean ± standard deviation and dot plot wherever appropriate. Except the data of Ki-67 staining, wound healing, and ^{1}H NMR, the individual controls were grouped to calculate the internal variation and all changes induced by treatments relative to the mean of controls of other measurements were calculated for statistical data analyses. Data were then further analyzed with Kruskal-Wallis test, followed by Dunn's test or one-way analysis of variance (ANOVA) followed by Dunnett test for comparison (GraphPad Prism 8.2.0, GraphPad Software, La Jolla, California, USA) wherever applicable. The gene data

in the two group were statistically analyzed with unpaired *t* test (if the effect size is large) or Mann-Whitney *U* test (if the effect size is small) [21,22]. A two-sided p value of<0.05 was considered to be a statistical significance. The NMR data were imported and processed by MATLAB R2018a (MathWorks, Cambridge, UK) programming language with MATLAB scripts [23,24]. After data was normalized with probabilistic quotient normalization method and aligned with recursive segment-wise peak alignment method, principal component analysis (PCA) and orthogonal projections to latent structures discriminant analysis (OPLS-DA) were used to analyze the processed spectral data [59,60]. The RNA array data was uploaded to GeneGlobe Data Analysis Centre (QIAGEN online program) and then analyzed.

Results

Effects of propofol on cancer malignancy in lung cancer and neuroglioma cells

Propofol decreased the cell viability of A549 cells (Fig. 1**A**) (NC *vs.* P of median [min–max range], 100.30% [93.74%, 104.7%] *vs.* 91.98% [89.02%, 94.63%], p < 0.001, n = 8), while there was no significant change in H4 cells (**Fig. S1A**; NC *vs.* P, p = 0.24, n = 8). A significant decrease of Ki-67 positive cell numbers was observed in A549 cells treated with propofol compared with the naïve control (Fig. 1**B and C**) (NC *vs.* P: 29.14% [21.87%, 51.64%] *vs.* 5.44% [5.12%, 7.33%], p < 0.05, n = 5). In contrast, no change was detected in H4 cells (**Fig. S1B and C**; p = 1.00 for NC *vs.* P, n = 5).

Propofol administration significantly decreased the migration of A549 cells (Fig. 1**D and E**) (NC *vs.* P: 55.38% [48.05%, 57.14%] *vs.* 23.56% [14.55%, 26.17%], p < 0.01, n = 5), but not H4 cells (**Fig. S1D and E**; p = 1.00 for NC *vs.* P, n = 5). As shown by Transwell assay, the invasion of A549 was significantly decreased (NC *vs.* P, 1.00 ± 0.14 *vs.* 0.67 ± 0.07, p < 0.01, n = 5) by propofol (Fig. 1**F** and **G**), while no significant difference (NC *vs.* P, p = 0.89, n = 5) in numbers of invasive cells following propofol administration was seen in H4 cells (**Fig. S1F** and **G**).

Propofol downregulated GLUT1 and MPC1 expressions in lung cancer cells but not in neuroglioma cells

The immunofluorescent staining of A549 cells showed GLUT1 (a cell membrane glucose transporter) and MPC1 (a mitochondrial pyruvate transporter) markers had clear co-expressions in naïve control group and vehicle control group, while both expressions in propofol group were significantly decreased (Fig. 2**A**). The protein expression levels of GLUT1 (0.29 ± 0.13 *vs.* 1.00 ± 0.69 of control, p < 0.05, n = 6) and MPC1 (0.55 ± 0.09 *vs.* 1.00 ± 0.16 of control, p < 0.01, n = 6) were significantly decreased by propofol treatment (Fig. 2**B-D**). In H4 cells, GLUT1 and MPC1 expressions had no significant changes among naïve control, vehicle control, and propofol groups in immunofluorescent staining (**Fig. S2A and B**) and Western blotting analysis (**Fig. S2C-F**) (NC *vs.* P, GLUT1, p = 0.74; MPC1, p = 0.99, n = 6).

Propofol disturbed the metabolism of lung cancer but not neuroglioma cells

The ^{1}H-NMR spectroscopy was used to analyze metabolic changes in cell extract and media samples of A549 and H4 cells. Pair-wise comparisons between control and propofol group of A549 and H4 cells were carried out using OPLS-DA analysis with one predictive component and one orthogonal component. R^2X, Q^2X, Q^2Y and permutation p values of OPLS-DA models were summarized in **Table S3**. The changes of metabolites observed in pairwise comparisons were shown in **Table S4**. It showed a clear separation in A549 cell extract samples between control and propofol groups (Fig. 2**E**). The significant difference was contributed by increased cellular concentrations of glutamate and glycine and decreased concentrations of formate and acetate in propofol group (Fig. 2**F**). The separation in media samples between control and propofol groups of A549 cells was also clear (Fig. 2**G**). With propofol treatment, the concentrations of glucose, lactate, glutamine, succinate, pyruvate, arginine, valine, isoleucine, leucine, glycerol and lipids were increased, while the concentrations of acetate, ethanol, and isopropanol were decreased (Fig. 2**H**). However, no significant metabolic differences between the propofol and the control groups in either H4 cells or media (permutation p values > 0.05).

Propofol increased PEDF expressions in lung cancer cells but not in neuroglioma cells

PEDF expression in A549 and H4 cells was evaluated using immunofluorescent staining and Western blotting. The immunofluorescent staining of A549 cells showed that the expression level of PEDF in propofol group was higher than naïve control group (Fig. 3**A**). A significant increase in PEDF protein in the propofol group was observed compared with naïve control group based on Western blotting analysis (NC *vs.* P, 1.00 ± 0.42 *vs.* 3.07 ± 1.95, p < 0.05, n = 6), but not between naïve and vehicle control groups in A549 cells (Fig. 3**E and F**). The immunofluorescent staining (**Fig. S3A**) and Western blotting analysis (**Fig. S3C and D**) of H4 cells showed no significant change between any groups analysis (NC *vs.* P, p = 0.37, n = 6).

Propofol suppressed both Akt and Erk pathways in lung cancer but not neuroglioma cells

Akt and Erk pathways, which could be affected by PEDF, were evaluated. The immunofluorescent staining showed both p-Akt (Fig. 3**B**) and p-Erk (Fig. 3**C**) of lung cancer cells were suppressed by propofol treatment. Western blotting analysis showed a significant decrease of p-Akt/Akt between the naïve control and propofol group (NC *vs.* P, 1.00 ± 0.45 *vs.* 0.35 ± 0.07, p < 0.01, n = 6) (Fig. 3**E** and **G**). Moreover, the evaluation for p-Erk/Erk showed the similar pattern that a significant change was identified between the naïve control and propofol group (NC *vs.* P, 1.00 ± 0.52 *vs.* 0.38 ± 0.07, p < 0.01, n = 6), but not between naïve and vehicle control group (Fig. 3**E** and **H**). In H4 cells, there was no significant change between any groups of p-Akt/Akt (NC *vs.* P, p = 1.00, n = 6, **Fig. S3C and E**) and p-Erk1/2 ratio Erk1/2 (NC *vs.* P, p = 0.72, n = 6, **Fig. S3C and F**).

HIF-1α expression was downregulated by propofol in lung cancer but not neuroglioma cells

HIF-1α is one of the downstream pathways of Akt and Erk pathways. The immunofluorescent staining showed HIF-1α expression in A549 cells was decreased after propofol treatment (Fig. 3**D**). HIF-1α expression in A549 cells measured by Western blotting was also decreased in the propofol group (0.67 ± 0.14, p < 0.01, n = 6) compared with the naïve control group (1.00 ± 0.20) (Fig. 3**E** and **I**). However, HIF-1α expression in H4 cells was not changed follow-

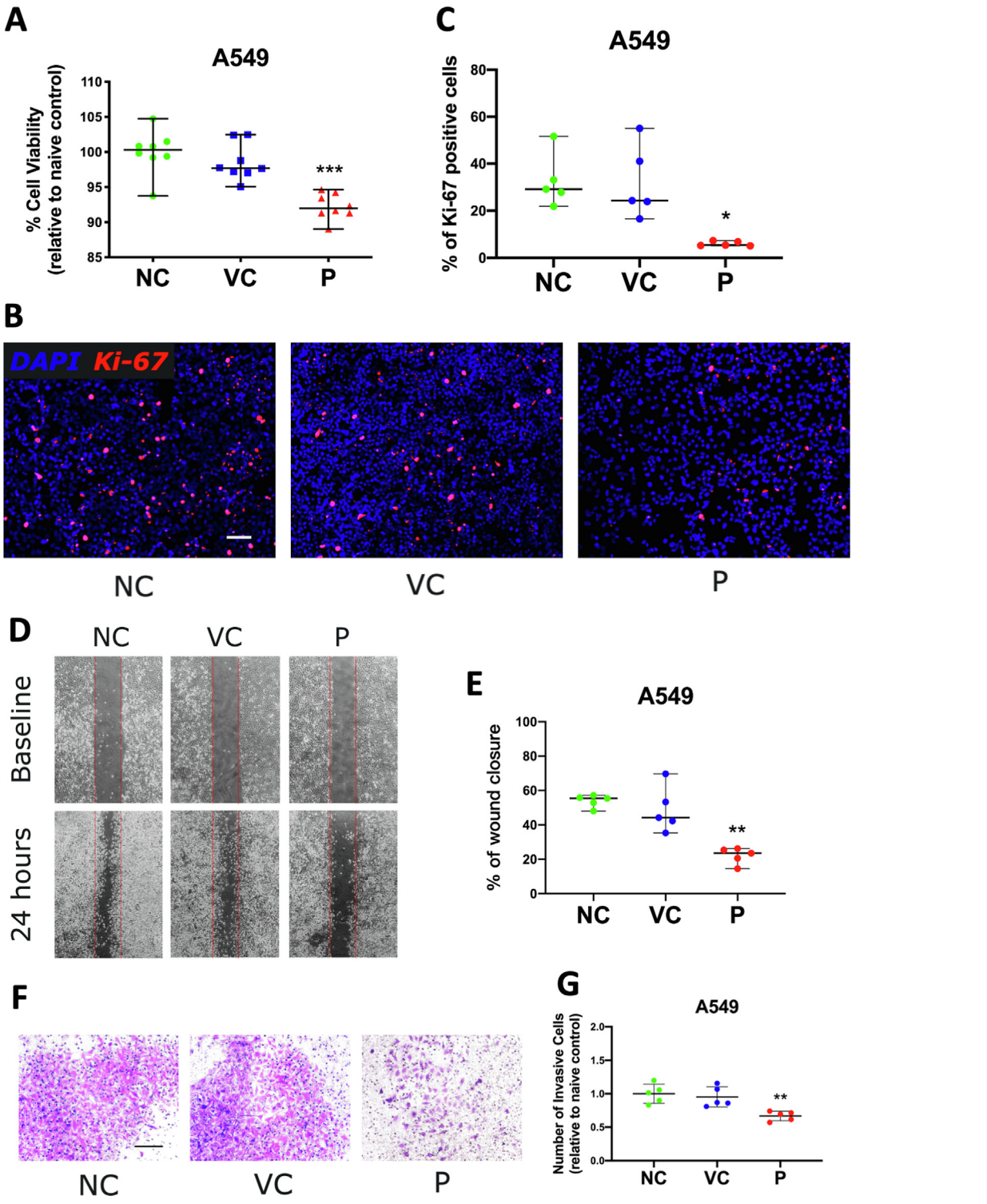

Fig. 1. The cell viability, proliferation, migration, and invasion of lung cancer cells after propofol exposure. Lung cancer (A549) cells were treated with intralipid (vehicle control), 4 μg/mL propofol, or pure culture media (naïve control). Cell viability of lung cancer cells was evaluated with the CCK-8 assay (**A**). Cell proliferative capability of A549 cells was evaluated with Ki-67 immunofluorescent staining (**B**) to compare the Ki-67 positive cell percentage in A549 cells (**C**). The migration was assessed *via* wound healing assay (**D**) with statistical analysis of the percentage of gap closure of A549 cells (**E**). The invasion of A549 cells (**F**) was evaluated by Transwell assay with the statistical analysis of the relative ratio of invasive cell number to NC (**G**). The data of CCK-8, Ki-67 staining, and wound healing assay were expressed as median with range and dot plot (n = 5–8). The data of Transwell assay was expressed as mean ± standard deviation and dot plot (n = 5). *p < 0.05, **p < 0.01, ***p < 0.001 versus naïve control. Scale bar: 100 μm. NC, naïve control; VC, vehicle control; P, propofol.

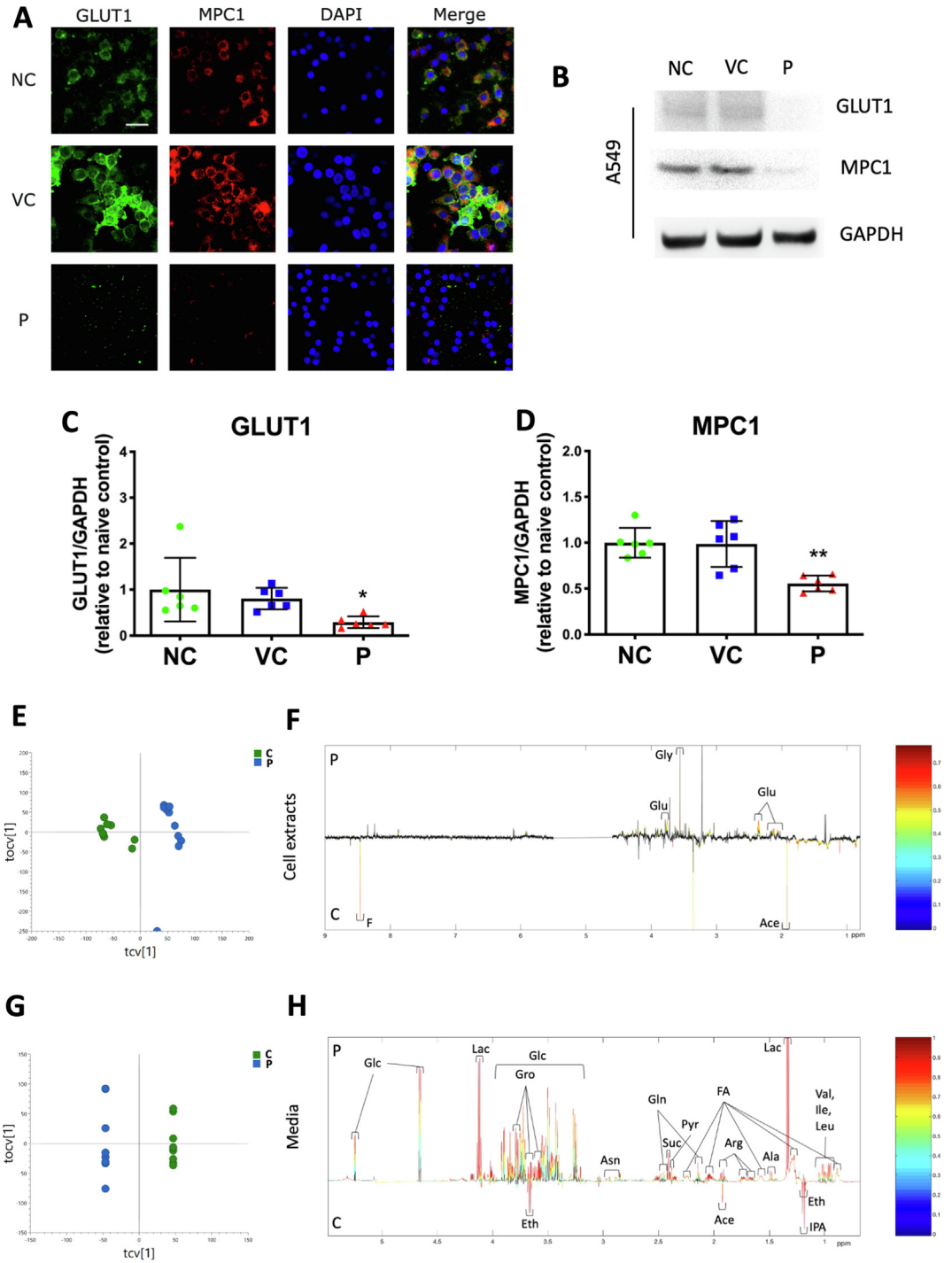

Fig. 2. Propofol disturbed cellular metabolism via down-regulating GLUT1 and MPC1 in lung cancer cells. Lung cancer A549 cells were administered with 4 μg/mL propofol or intralipid (vehicle control) or media without drugs (naïve control) for 2 h followed by 24 h recovery time. GLUT1 (green) and MPC1 (red) expressions were identified by dual-immunofluorescent staining (**A**). The expression levels of GLUT1 and MPC1 were validated with Western blotting analysis (**B-D**). The intensity of Western blotting bands was normalized by housekeeping protein GAPDH. Data were analyzed with one-way analysis of variance (ANOVA) followed by Dunnett multi-comparison test. Data were presented as mean ± standard deviation and dot plot (n = 6). Orthogonal projection to latent structures-discriminant analysis (OPLS-DA) loadings plots from ^{1}H NMR spectral data of the A549 cell extract (**E** and **F**) and media samples (**G** and **H**) for comparisons as control *vs.* propofol (n = 9–10). **E** and **G**: OPLS-DA scores plot; **F** and **H**: OPLS-DA loadings plot. The color bar indicates the correlation coefficient values (r^2) to be high in red and low in blue. *p < 0.05; **p < 0.01 versus naïve control. Scale bar: 50 μm. Metabolites and r^2 value were presented below, F: formate (0.58); Glc: glucose (0.90); Gln: Glutamine (0.83); Glu: glutamate (0.67); Eth: ethanol (0.98); Gly: glycine (0.58); Suc: succinate (0.98); Pyr: pyruvate (0.81); Ace: acetate (0.62); Arg: arginine (0.94); Lac: lactate (0.74); Gro: glycerol (0.98); FA: fatty acids (0.86); IPA: isopropanol (0.61); Val: valine (0.49); Ile: isoleucine (0.98); Leu: leucine (0.79). NC: naïve control; VC: vehicle control; P: propofol; C: control; GLUT1: glucose transporter 1; MPC1: mitochondrial pyruvate carrier 1.

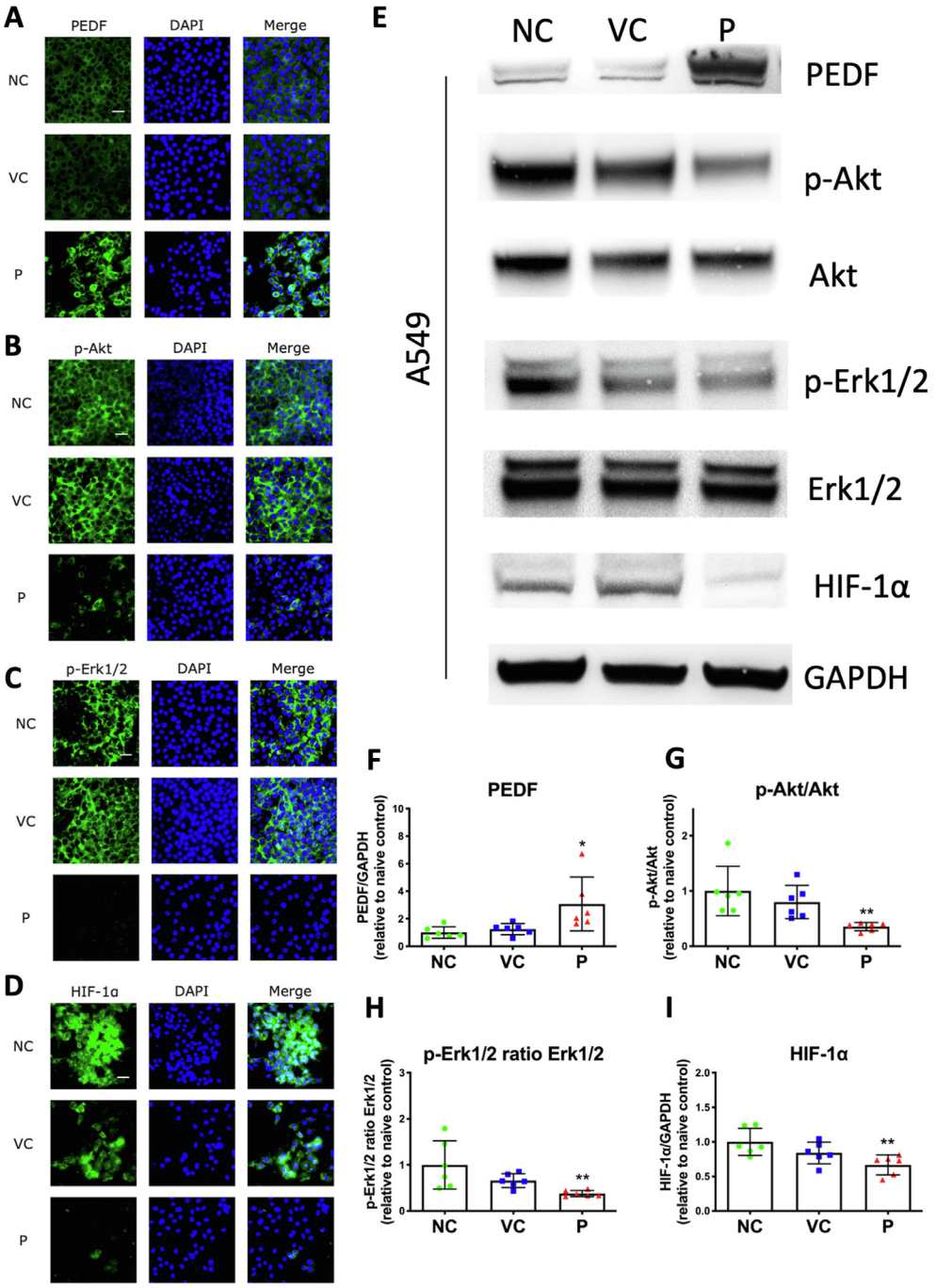

Fig. 3. Propofol up-regulated PEDF and down-regulated p-Akt/Akt, p-Erk1/2 ratio Erk1/2, and HIF-1α in lung cancer cells. Lung cancer (A549) cells were administered with a clinically relevant concentration 4 μg/mL of propofol for 2 h. The expression of PEDF (**A**), p-Akt (**B**), p-Erk (**C**), and HIF-1α (**D**) was analyzed by immunofluorescent staining. The target protein (green) was overlaid with DAPI (blue). The expression levels of PEDF, p-Akt, Akt, p-Erk1/2, Erk1/2, HIF-1α, and GAPDH were analyzed by Western blotting (**E**). The intensity of Western blotting bands was normalized by housekeeping protein GAPDH (**F-I**). Data were analyzed with one-way analysis of variance (ANOVA) followed by Dunnett multi-comparison test. Data were presented as mean ± standard deviation and dot plot (n = 6). *p < 0.05, **p < 0.01 versus naïve control. Scale bar: 50 μm. NC: naïve control; VC: vehicle control; P: propofol; PEDF: pigment epithelium-derived factor; p-Akt: phospho-Akt; Erk1/2: extracellular-signal-regulated kinase 1/2; p-Erk1/2: phospho-Erk 1/2; HIF-1α: hypoxia-inducible factor-1 alpha.

ing propofol exposure (**Fig. S3C** and **G**) (p = 0.91 for NC *vs*. P of Western blotting analysis, n = 6).

Effects of propofol on tumor-related gene expressions of lung cancer and neuroglioma cells

Out of 84 tumor-related genes, 6 pro-tumor genes, namely, *VEGFA, CTBP1, CST7, CTSK, CXCL12, and CXCR4,* were downregulated in the propofol group compared with control. In addition, 8 anti-tumor genes including *NR4A3, RB1, NME1, MTSS1, NME4, SYK, APC, and FAT1* were upregulated (Fig. 4**A**) in lung cancer cells. Among these altered gene expressions (summarized in **Table S5**), *CXCR4* were significantly downregulated by propofol administration (Fig. 4**B**, *CXCR4*, C *vs.* P, 1.000 ± 0.004 *vs.* 0.986 ± 0.004, p < 0.05, n = 3). The similar changes were subsequently validated by qRT-PCR (Fig. 4**C**) (0.23 ± 0.16 *vs.* 1.00 ± 0.41 of control,

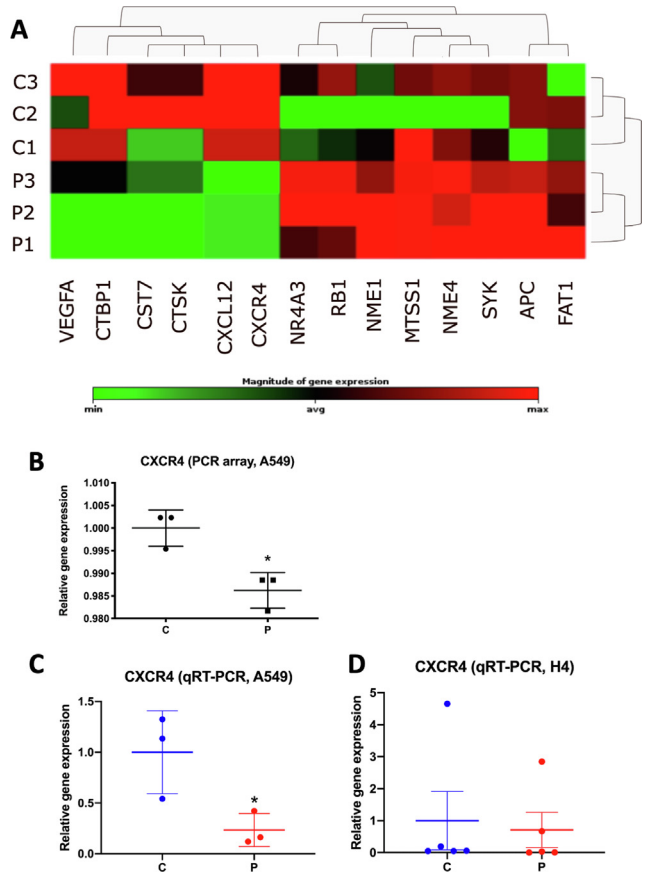

Fig. 4. Propofol altered lung cancer cell mRNA expression levels of tumor-related genes assessed by PCR array and qRT-PCR. Lung cancer (A549) cells were treated with 4 μg/mL propofol or intralipid as the control for 2 h and then recovered for up to 24 h. **A**. The PCR array analysis of tumor-related genes. Unsupervised hierarchical cluster analysis using Euclidean distance from the low-density arrays. Propofol upregulated 8 anti-tumor genes and downregulated 6 pro-tumor genes of A549 cells (n = 3). The data is relative to endogenous control, GAPDH. Red and green colors indicate relatively high and low expression, respectively. The results of *CXCR4* obtained from A549 cells using PCR array (**B**, n = 3) and qRT-PCR (**C**, n = 3) were presented. The result of *CXCR4* obtained from H4 cells using qRT-PCR was presented (**D**, n = 5). Data were expressed as mean ± standard deviation and dot plot. $^{*}p < 0.05$ versus control. C: control; P: propofol; *VEGFA*: vascular endothelial growth factor A; *CTBP1*: C-terminal binding protein 1; *CST7*: cystain 7; *CTSK*: cathepsin K; *CXCL12*: C-X-C motif chemokine 12; *CXCR4*: C-X-C chemokine receptor type 4; *NR4A3*: nuclear receptor subfamily 4 group A member 3; *RB1*: retinoblastoma susceptility 1; *NME1*: NME/NM23 nucleoside diphosphate kinase 1; *MTSS1*: metastasis suppressor I-BAR domain containing 1; *NME4*: NME/NM23 nucleoside diphosphate kinase 4; *SYK*: spleen tyrosine kinase; *APC*: adenomatous polyposis coli; *FAT1*: FAT tumor suppressor homolog 1.

$p < 0.05$, n = 3). However, there was no significant change in *CXCR4* expression (Fig. 4**D**, p = 0.42, n = 5) in H4 cells between control and propofol groups.

The statistical values of CCK-8 assay, Ki-67 staining, would healing assay, Transwell assay, Western blot, PCR array and qRT-PCR experiment were also summarized in **Table S6.**

Discussion

In the current study, we found that propofol, one of the most commonly used intravenous general anesthetic, downregulated GLUT1, MPC1, HIF-1α, p-Akt and p-Erk1/2 expressions and upregulated PEDF in lung cancer cells but not in brain cancer cells (Fig. 5). Furthermore, 6 pro-tumor genes were downregulated and 8 anti-tumor genes were upregulated after propofol administration, while the cell metabolism of lung cancer cells was altered by propofol. Ultimately, the cell viability, proliferation, migration and invasion of lung cancer cells were suppressed by propofol. However, these effects of propofol were not found in neuroglioma cells. Our data indicated that the malignancy of lung cancer cells was attenuated by propofol, which might be associate with the alterations of cell metabolisms and cell signaling pathways.

In this study, propofol was found to inhibit GLUT1 and MPC1 expressions, which were located at the cellular and mitochondrial membrane, respectively. In line with our data, propofol was previously reported to suppress GLUT1 expression in human myeloid leukemia cells [25]. MPC1 is responsible for transferring pyruvate into mitochondria for the tricarboxylic acid (TCA) cycle, which is a major energy synthesis pathway for normal cells [26]. However, in contrast to normal cells, cancer cells are more likely to shift from mitochondrial oxidative phosphorylation to glycolysis, such phenomenon is called "Warburg effect" [27]. "Warburg effect" requires the downregulation of MPC1 in cancer cells and the MPC1 levels are relatively low in several cancer types, including lung cancer [28,29]. Although cancer cells do not mainly rely on the TCA cycle to generate ATP, it still requires the TCA cycle to produce the intermediates for the synthesis of nucleic acids, fatty acids, and carbon skeleton [30]. However, MPC1 deficiency was reported to increase the malignancy of lung adenocarcinoma *via* STAT3 pathway [29]. This discrepancy between that study and ours remains to be investigated, but in most of cancer types including lung cancer, the glucose uptake was increased by upregulating GLUT1 level [31]. Our data showed that both MPC1 and GLUT1 expression were downregulated by propofol exposure, indicating that the malignancy of the lung cells used in our study was suppressed *via* cell metabolism by propofol, but this warrants further study.

Interestingly, resveratrol is a phenolic structured natural healthy supplement that not only blocks the activity of GLUT1, but also downregulates the expression level of GLUT1. It was found that the exposure of resveratrol to leukemic and ovarian cancer cells inhibits the uptake of glucose [32]. Resveratrol was found to inhibit the proliferation, metastasis and epigenetic alterations, and induce the apoptosis *in vitro* and *in vivo* studies of breast cancer [33]. Lonidamine, an anti-tumor drug, was found to kill cancer cells by inhibiting the activity of MPC1. This was in agreement with our ^{1}H NMR spectral data, which showed that pyruvate, lactate and glucose in the media of lung cancer cells was increased by propofol, indicating that glucose uptake was inhibited and pyruvate was more converted to lactate and less entered the TCA cycle. This was very likely due to the decrease of MPC1 demonstrated in our study while propofol itself induced mitochondrial bilayer perturbations might contribute to this. In cancer cells, pyruvate is converted to formate and acetyl-CoA catalyzed by pyruvate formate lyase, and acetyl-CoA can be metabolized to acetate or enter TCA cycle [34]. The concentrations of formate and acetate were decreased following the administration of propofol, indicating pyruvate metabolism towards the production of acetyl-CoA was reduced. In cancer cells, apart from glucose, glutamine is another nutrition source, which is converted to glutamate and used in TCA cycle, namely glutaminolysis [35]. Our data showed that the concentration of glutamine and glutamate was increased in media and lung cancer cell extracts respectively after treated with propofol, which was an evidence of lower activity of glutaminolysis and TCA cycle. The metabolism of other amino acids was also affected, including glycine, succinate,

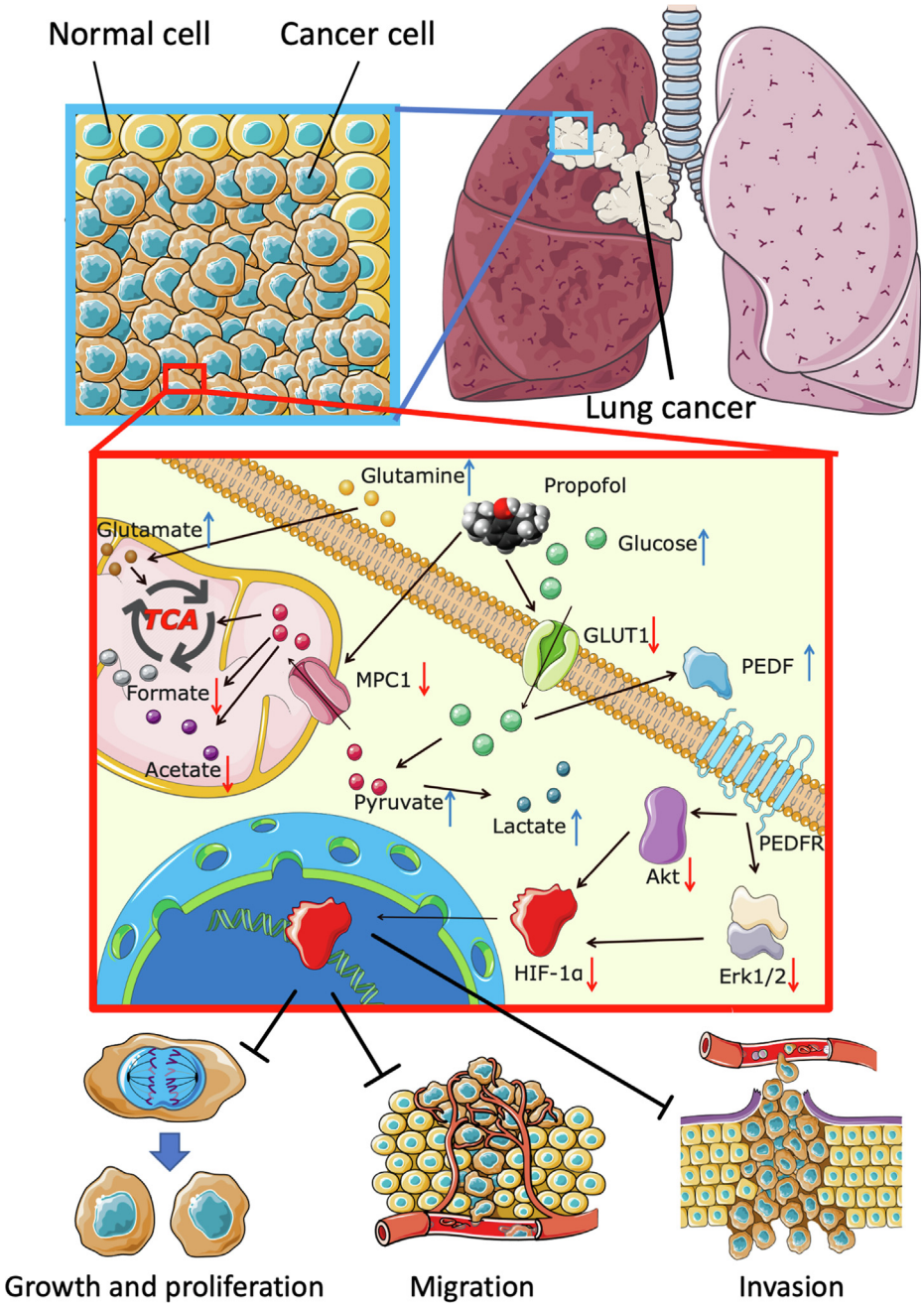

Fig. 5. The cellular signaling interactions in lung cancer cells after propofol administration. Propofol downregulates GLUT1, which decreases glucose uptake into cell plasma. Propofol also downregulates MPC1 expression, which converts pyruvate more to lactate and less to formate and acetate or enters TCA cycle. The decreased level of TCA activity uses less glutamate, which inhibits the uptake of glutamine. Furthermore, the decreased activation of TCA cycle inhibits the generation of intermediates for the synthesis of nucleic acids, fatty acids, and carbon skeleton. The less uptake of glucose induces the secretion of PEDF. PEDF inhibits both Akt and Erk phosphorylation, which leads to the downregulation of HIF-1α. HIF-1α is less translocated into the nucleus and increases anti-tumor genes or decreases pro-tumor genes. Propofol disturbs metabolism and alters tumor-related genes and ultimately inhibits the malignancy of lung cancer cells. GLUT1: glucose transporter 1; MPC1: mitochondrial pyruvate carrier 1; TCA: tricarboxylic acid; PEDF: pigment epithelium-derived factor; Erk1/2: extracellular signal-regulated kinase 1/2; HIF-1α: hypoxia-inducible factor 1 alpha.

arginine, valine, isoleucine, and leucine. Glycine was elevated in lung cancers administered with propofol as glycine can be converted to pyruvate, which is relevant with glucose metabolism or TCA cycle [36]. Isoleucine, leucine, valine, succinate, and arginine was elevated in the media of propofol group, which further indicted that propofol inhibited the metabolism of lung cancer cells, leading to less utilization of amino acids. Isopropanol, a potential primary lung cancer biomarker [37], was decreased in lung cancer cells with propofol treatment, suggesting that the progression of lung cancer cells was inhibited by the treatment. Although the metabolism of isopropanol was not fully understood, some reports claimed that isopropanol might be transformed from acetone, which was converted from pyruvate [38,39]. Another source of acetone is from beta-oxidation of fatty acids in mitochon-

dria [40]. Propofol might injure mitochondrial beta-oxidation, which generated less acetone to convert to isopropanol. These findings collectively indicated that propofol likely causes mitochondrial injury and disturbs cancer cell metabolisms. One can argue that propofol may be also harmful to normal cells and even patients. Indeed, propofol infusion syndrome occurs when some patients are administered with a high dose infusion of propofol for more than 48 h [41], which was reported to be related to mitochondrial injury such as oxidative phosphorylation defect [42,43]. It is true that propofol is different from other anesthetics as it has a unique phenolic structure, which gives it a lipophilic property that can be solubilized inside the lipid membrane bilayer and induce the lipid perturbations [44,45], whilst the lipid bilayer is the platform for protein–protein interaction and cellular signaling modulation, and its perturbations can affect several signaling pathways and biochemical reactions [46]. Therefore, compared to normal cells, cancer cells are more vulnerable to propofol, which decreases the malignancy of cancer cells without harm to normal cells and patients during cancer surgery for relatively short time use.

It was reported that with higher glucose uptake, PEDF expression was decreased in retinal Muller cells [47,48]. In line with this, GLUT1 was downregulated in lung cancer cells by propofol and less glucose was transferred into lung cancer cells. It was consistent with our finding of elevated glucose in media, which might suggest less glucose was utilized by cells. This might induce the secretion of PEDF, which was confirmed with our both immunofluorescent staining and Western blot data (Fig. 3). PEDF has an anti-tumor and anti-angiogenesis property and some tumor malignancy-related cellular signaling pathways in lung cancer cells may likely be interrupted by the increased level of PEDF. Indeed, Akt and Erk in lung cancer cells were inhibited by propofol as shown in our study and also reported previously [49,50]. Our group previously demonstrated that volatile anesthetic isoflurane enhanced the malignancy of renal cancer cells by activating HIF-1α *via* Akt signaling pathway [51]. Overexpressed HIF-1α had been found in many aggressive cancer types and was found to correlate with tumor progression [52,53]. In contrast to inhaled anesthetics, propofol inactivated HIF-1α in lung cancer cells in the current study; this is consistent with prostate cancer cells in which propofol inhibited the synthesis of HIF-1α through Akt pathway which was initially induced by isoflurane and then suppressed by the superposition of propofol as we reported [11]. HIF-1α is a key transcriptional regulator which are involved in cell survival, proliferation, migration and invasion [54]. Our PCR array results showed that several pro-tumor genes (for example, *VEGFA, CXCL12*, and *CXCR4*) were downregulated and anti-tumor genes (for example, *RB1, APC,* and *FAT1*) were upregulated (**Table S5**). These were in contrast to volatile anesthetics which induced the tumor metastatic related genes that were associated with the enhanced malignancy of ovarian cancer cells [10]. Interestingly, a retrospective clinical study showed that patients received tumor resection were grouped into total intravenous anesthesia (propofol and remifentanil) or inhalational anesthesia (isoflurane or sevoflurane) groups. It was found that patients received inhalational anesthesia during cancer surgery had a lower 3 year-survival rate than those received propofol-based intravenous anesthesia [9]. In another study, it was concluded that propofol-based intravenous anesthesia for colonic cancer surgery was associated with better survival rate than desflurane-based inhalational anesthesia [55]. Arguably, these clinical data are well supported by our current findings that propofol inhibits the malignancy of cancer cells, albeit derived from lung cancer.

In contrast, the expressions of GLUT1, MPC1, PEDF, p-Akt, p-Erk, and HIF-1α were not changed in neuroglioma cells by propofol. In addition, no significant changes were identified in our metabolism and PCR data. Unlike lung cancer cells, the cell viability, proliferation, migration, and invasion of neuroglioma cells were not significantly inhibited by propofol either. Why neuroglioma cells behaved so different to propofol compared to lung cancer cells is unknown and warrants further study. One can argue that, in general, brain cancer is very insensitive to chemotherapy and/or radiotherapy, indicating that this type of cancer is more robust than other cancer types. Nevertheless, our study may support clinical retrospective observations, in which patients were under either propofol or sevoflurane maintenance of anesthesia for glioma resection and their progression-free or overall survival were not different between two anesthetic regimens [56,57]. The current study was based on *in vitro* assays and the future investigation need to be carried out *in vivo* to evaluate the effect of propofol at the systemic level. Clinically, there are many other risk factors, for example, surgery induced inflammation and abnormal immune function during perioperative period, that also affect the prognosis of cancer patients after surgery. It was reported that propofol increased the cytotoxicity effects of natural killer (NK) cells, which might also benefit the outcome of cancer patients [58]. All these point to that propofol may be a good choice of anesthetics used during surgery for certain cancer type but in order to better simulate clinical scenarios, *in vivo* and clinical studies are required.

Conclusion

Our data suggested that unlike brain cancer cells, propofol disturbed the metabolism, decreased GLUT1 and MPC1 expressions, and increased PEDF expression of lung cancer cells. PEDF then inhibited HIF-1α *via* both Akt and Erk signaling and consequently upregulated anti-tumor genes and downregulated pro-tumor genes. The alteration of tumor-related genes together with the disturbance of cellular metabolism may ultimately lead to the inhibition of malignancy of lung cancer cells. Our study likely leads to new anesthetic regimens for lung cancer surgery to reduce lung cancer post-surgical recurrent risk. However, *in vitro* experimental setting cannot represent clinical scenario and, therefore, further clinical study/trial are required to valid the benefit effects of propofol found in our study.

Declaration of Competing Interest

The authors declared that there is no conflict of interest.

Acknowledgements

CH, MI, ZL and BW: Perform experiments and analyzed data. XL, HL and JL: Participated experiments. JVL, QL and DM: Designed experiments. All authors interpreted data and wrote manuscript. This work and the authors were supported by China Scholarship Council, Beijing, China (201700260043, 2017-2020); Medical Research Council, London, UK (MR/P002536/1); European Research Council (715662); Royal College of Anaesthetists, London, UK; and the Second Affiliated Hospital and Yuying Children's Hospital of Wenzhou Medical University, Wenzhou, Zhejiang, China. Fig. 5 was created by using Servier Medical Art materials, which are licensed under a Creative Commons Attribution 3.0 Unported License.

Appendix A. Supplementary data

Supplementary data to this article can be found online at https://doi.org/10.1016/j.jare.2020.12.007.

References

[1] Collaboration GBoDC. Global, Regional, and National Cancer Incidence, Mortality, Years of Life Lost, Years Lived With Disability, and Disability-Adjusted Life-years for 32 Cancer Groups, 1990 to 2015: A Systematic Analysis for the Global Burden of Disease Study. JAMA oncology. 2017;3(4):524-48.

[2] Torre LA, Bray F, Siegel RL, Ferlay J, Lortet-Tieulent J, Jemal A. Global Cancer Statistics, 2012. Ca-a Cancer Journal for Clinicians. 2015;65(2):87–108.

[3] Siegel RL, Miller KD, Jemal A. Cancer Statistics, 2017. Ca-a Cancer J Clinicians 2017;67(1):7–30.

[4] A new clinical guideline from the Royal College of Paediatrics and Child Health with a national awareness campaign accelerates brain tumor diagnosis in UK children–"HeadSmart: Be Brain Tumour Aware". Neuro-oncology. 2016;18(3):445-54.

[5] Aliperti LA, Predina JD, Vachani A, Singhal S. Local and systemic recurrence is the Achilles heel of cancer surgery. Ann Surg Oncol 2011;18(3):603–7.

[6] Ng JCH, See AAQ, Ang TY, Tan LYR, Ang BT, King NKK. Effects of surgery on neurocognitive function in patients with glioma: a meta-analysis of immediate post-operative and long-term follow-up neurocognitive outcomes. J Neurooncol 2019;141(1):167–82.

[7] Lee JS, Kim SI, Park HS, Lee JS, Park S, Park BW. The impact of local and regional recurrence on distant metastasis and survival in patients treated with breast conservation therapy. J Breast Cancer 2011;14(3):191–7.

[8] Horowitz M, Neeman E, Sharon E, Ben-Eliyahu S. Exploiting the critical perioperative period to improve long-term cancer outcomes. Nat Rev Clin Oncol 2015;12(4):213–26.

[9] Wigmore TJ, Mohammed K, Jhanji S. Long-term Survival for Patients Undergoing Volatile versus IV Anesthesia for Cancer Surgery: A Retrospective Analysis. Anesthesiology 2016;124(1):69–79.

[10] Iwasaki M, Zhao H, Jaffer T, Unwith S, Benzonana L, Lian Q, et al. Volatile anaesthetics enhance the metastasis related cellular signalling including CXCR2 of ovarian cancer cells. Oncotarget. 2016;7(18):26042–56.

[11] Huang H, Benzonana LL, Zhao H, Watts HR, Perry NJ, Bevan C, et al. Prostate cancer cell malignancy via modulation of HIF-1alpha pathway with isoflurane and propofol alone and in combination. Br J Cancer 2014;111(7):1338–49.

[12] Soni S, Padwad YS. HIF-1 in cancer therapy: two decade long story of a transcription factor. Acta oncologica (Stockholm, Sweden). 2017;56(4):503–15.

[13] Jing Y, Liu LZ, Jiang Y, Zhu Y, Guo NL, Barnett J, et al. Cadmium increases HIF-1 and VEGF expression through ROS, ERK, and AKT signaling pathways and induces malignant transformation of human bronchial epithelial cells. Toxicological sciences : an official J Society Toxicology 2012;125(1):10–9.

[14] Wan J, Wu W. Hyperthermia induced HIF-1a expression of lung cancer through AKT and ERK signaling pathways. J experimental clinical cancer research : CR. 2016;35(1):119.

[15] Mayer IA, Arteaga CL. The PI3K/AKT Pathway as a Target for Cancer Treatment. Annu Rev Med 2016;67:11–28.

[16] Samatar AA, Poulikakos PI. Targeting RAS-ERK signalling in cancer: promises and challenges. Nat Rev Drug Discovery 2014;13(12):928–42.

[17] Yuan Y, Liu X, Miao H, Huang B, Liu Z, Chen J, et al. PEDF increases GLUT4-mediated glucose uptake in rat ischemic myocardium via PI3K/AKT pathway in a PEDFR-dependent manner. Int J Cardiol 2019;283:136–43.

[18] Sanchez A, Tripathy D, Yin X, Luo J, Martinez J, Grammas P. Pigment epithelium-derived factor (PEDF) protects cortical neurons in vitro from oxidant injury by activation of extracellular signal-regulated kinase (ERK) 1/2 and induction of Bcl-2. Neurosci Res 2012;72(1):1–8.

[19] Conte MI, Cabrillana ME, Saez Lancellotti TE, Simon L, Funes AK, Cayado-Gutierrez N, et al. Pigment epithelium derived factor (PEDF) expression in the male tract of Wistar rats. Biochem Biophys Res Commun 2018;504(1):257–62.

[20] Wei Y, Elahy M, Friedhuber AM, Wong JY, Hughes JD, Doschak MR, et al. Triple-threat activity of PEDF in bone tumors: Tumor inhibition, tissue preservation and cardioprotection against doxorubicin. Bone 2019;124:103–17.

[21] De Winter JC. Using the Student's t-test with extremely small sample sizes. Practical Assessment, Research Evaluation 2013;18(1):10.

[22] Cohen J. Statistical power analysis for the behavioral sciences. Academic press; 2013.

[23] Trygg J, Holmes E, Lundstedt T. Chemometrics in metabonomics. J Proteome Res 2007;6(2):469–79.

[24] Haggart GA. csmsoftware/IMPaCTS: Version 1.1.1 (Version v1.1.1) Zenodo2019 [Available from: http://doi.org/10.5281/zenodo.3077413.

[25] Tanaka T, Takabuchi S, Nishi K, Oda S, Wakamatsu T, Daijo H, et al. The intravenous anesthetic propofol inhibits lipopolysaccharide-induced hypoxia-inducible factor 1 activation and suppresses the glucose metabolism in macrophages. J anesthesia 2010;24(1):54–60.

[26] Bricker DK, Taylor EB, Schell JC, Orsak T, Boutron A, Chen Y-C, et al. A mitochondrial pyruvate carrier required for pyruvate uptake in yeast, Drosophila, and humans. Science 2012;337(6090):96–100.

[27] Vander Heiden MG, Cantley LC, Thompson CB. Understanding the Warburg effect: the metabolic requirements of cell proliferation. Science 2009;324(5930):1029–33.

[28] Lu Y, Yi Y, Liu P, Wen W, James M, Wang D, et al. Common human cancer genes discovered by integrated gene-expression analysis. PloS one. 2007;2(11):e1149-e.

[29] Zou H, Chen Q, Zhang A, Wang S, Wu H, Yuan Y, et al. MPC1 deficiency accelerates lung adenocarcinoma progression through the STAT3 pathway. Cell death & disease. 2019;10(3):148-.

[30] Anderson NM, Mucka P, Kern JG, Feng H. The emerging role and targetability of the TCA cycle in cancer metabolism. Protein Cell. 2018;9(2):216–37.

[31] Pezzuto A, D'Ascanio M, Ricci A, Pagliuca A, Carico E. Expression and role of p16 and GLUT1 in malignant diseases and lung cancer: A review. Thorac Cancer 2020.

[32] Zambrano A, Molt M, Uribe E, Salas M. Glut 1 in Cancer Cells and the Inhibitory Action of Resveratrol as A Potential Therapeutic Strategy. Int J Mol Sci 2019;20(13).

[33] Sinha D, Sarkar N, Biswas J, Bishayee A. Resveratrol for breast cancer prevention and therapy: Preclinical evidence and molecular mechanisms. Semin Cancer Biol 2016;40–41:209–32.

[34] Tack I, Nimmegeers P, Akkermans S, Logist F, Van Impe JFM. A low-complexity metabolic network model for the respiratory and fermentative metabolism of Escherichia coli. PLoS ONE 2018;13(8):e0202565.

[35] Dang CV. Glutaminolysis: supplying carbon or nitrogen or both for cancer cells?. Cell cycle (Georgetown, Tex). 2010;9(19):3884–6.

[36] Cheng ZX, Guo C, Chen ZG, Yang TC, Zhang JY, Wang J, et al. Glycine, serine and threonine metabolism confounds efficacy of complement-mediated killing. Nat Commun 2019;10(1):3325.

[37] Wehinger A, Schmid A, Mechtcheriakov S, Ledochowski M, Grabmer C, Gastl GA, et al. Lung cancer detection by proton transfer reaction mass-spectrometric analysis of human breath gas. Int J Mass Spectrom 2007;265(1):49–59.

[38] Lewis GD, Laufman AK, McAnalley BH, Garriott JC. Metabolism of acetone to isopropyl alcohol in rats and humans. J Forensic Sci 1984;29(2):541–9.

[39] Li WW, Liu Y, Liu Y, Cheng SQ, Duan YX. Exhaled isopropanol: new potential biomarker in diabetic breathomics and its metabolic correlations with acetone. RSC Adv 2017;7(28):17480–8.

[40] Laffel L. Ketone bodies: a review of physiology, pathophysiology and application of monitoring to diabetes. Diabetes Metab Res Rev 1999;15(6):412–26.

[41] Mirrakhimov AE, Voore P, Halytskyy O, Khan M, Ali AM. Propofol infusion syndrome in adults: a clinical update. Crit Care Res Pract 2015;2015:260385.

[42] Sumi C, Okamoto A, Tanaka H, Nishi K, Kusunoki M, Shoji T, et al. Propofol induces a metabolic switch to glycolysis and cell death in a mitochondrial electron transport chain-dependent manner. PLoS ONE 2018;13(2):e0192796.

[43] Vanlander AV, Jorens PG, Smet J, De Paepe B, Verbrugghe W, Van den Eynden GG, et al. Inborn oxidative phosphorylation defect as risk factor for propofol infusion syndrome. Acta Anaesthesiol Scand 2012;56(4):520–5.

[44] Reitz M, Velizarov S, Glück B, Berg H, Brambrink AM. Effects of propofol (intravenous propofol emulsion) on cell membrane measures by electrofusion and electroporation. Arzneim-Forsch 1999;49(3):281–5.

[45] Bahri MA, Seret A, Hans P, Piette J, Deby-Dupont G, Hoebeke M. Does propofol alter membrane fluidity at clinically relevant concentrations? An ESR spin label study. Biophys Chem 2007;129(1):82–91.

[46] Hicks DA, Nalivaeva NN, Turner AJ. Lipid rafts and Alzheimer's disease: protein-lipid interactions and perturbation of signaling. Front Physiol 2012;3:189.

[47] Mu H, Zhang X-M, Liu J-J, Dong L, Feng Z-L. Effect of high glucose concentration on VEGF and PEDF expression in cultured retinal Müller cells. Mol Biol Rep 2009;36(8):2147.

[48] Yamagishi S-i, Matsui T. Pigment epithelium-derived factor (PEDF) and cardiometabolic disorders. Curr Pharm Des 2014;20(14):2377–86.

[49] Hsing C-H, Lin M-C, Choi P-C, Huang W-C, Kai J-I, Tsai C-C, et al. Anesthetic propofol reduces endotoxic inflammation by inhibiting reactive oxygen species-regulated Akt/IKKβ/NF-κB signaling. PLoS ONE 2011;6(3):e17598.

[50] Fibuch EE, Wang JQ. Inhibition of the MAPK/ERK cascade: a potential transcription-dependent mechanism for the amnesic effect of anesthetic propofol. Neuroscience bulletin. 2007;23(2):119–24.

[51] Benzonana LL, Perry NJ, Watts HR, Yang B, Perry IA, Coombes C, et al. Isoflurane, a commonly used volatile anesthetic, enhances renal cancer growth and malignant potential via the hypoxia-inducible factor cellular signaling pathway in vitro. Anesthesiology 2013;119(3):593–605.

[52] Unwith S, Zhao H, Hennah L, Ma D. The potential role of HIF on tumour progression and dissemination. International journal of cancer Journal international du cancer. 2015;136(11):2491–503.

[53] Zhao H, Iwasaki M, Yang J, Savage S, Ma D. Hypoxia-inducible factor-1: a possible link between inhalational anesthetics and tumor progression?. Acta anaesthesiologica Taiwanica : official journal of the Taiwan Society of Anesthesiologists. 2014;52(2):70–6.

[54] Semenza GL. Targeting HIF-1 for cancer therapy. Nat Rev Cancer 2003;3(10):721–32.

[55] Wu ZF, Lee MS, Wong CS, Lu CH, Huang YS, Lin KT, et al. Propofol-based Total Intravenous Anesthesia Is Associated with Better Survival Than Desflurane Anesthesia in Colon Cancer Surgery. Anesthesiology 2018;129(5):932–41.
[56] Dong J, Zeng M, Ji N, Hao S, Zhou Y, Gao Z, et al. Impact of Anesthesia on Long-term Outcomes in Patients With Supratentorial High-grade Glioma Undergoing Tumor Resection: A Retrospective Cohort Study. J Neurosurg Anesthesiol 2020;32(3):227–33.
[57] Saito J, Masters J, Hirota K, Ma D. Anesthesia and brain tumor surgery: technical considerations based on current research evidence. Current opinion in anaesthesiology. 2019;32(5):553–62.
[58] Li R, Liu H, Dilger JP, Lin J. Effect of Propofol on breast Cancer cell, the immune system, and patient outcome. BMC anesthesiology. 2018;18(1):77.
[59] Veselkov Kiril A Lindon et al. Recursive segment-wise peak alignment of biological 1H NMR spectra for improved metabolic biomarker recovery. Analytical chemistry 2009;81(1):56–66.
[60] Dieterle Frank Ross et al. Probabilistic quotient normalization as robust method to account for dilution of complex biological mixtures. Application in 1H NMR metabonomics. Analytical chemistry 2006;78(13):4281–90.